C. R. Mecanique 346 (2018) 439–448

Contents lists available at ScienceDirect

Comptes Rendus Mecanique

www.sciencedirect.com

Hybrid continuum–coarse-grained modeling of erythrocytes

Jinming Lyu [a], Paul G. Chen [a,*], Gwenn Boedec [b], Marc Leonetti [c], Marc Jaeger [a]

[a] Aix Marseille Univ, CNRS, Centrale Marseille, M2P2, Marseille, France
[b] Aix Marseille Univ, CNRS, Centrale Marseille, IRPHE, Marseille, France
[c] Université Grenoble Alpes, CNRS, LRP, Grenoble, France

ARTICLE INFO

Article history:
Received 13 November 2017
Accepted 22 April 2018
Available online 1 May 2018

Keywords:
Lipid membrane
Vesicle dynamics
Red blood cell
Boundary element method
Stokes flow

ABSTRACT

The red blood cell (RBC) membrane is a composite structure, consisting of a phospholipid bilayer and an underlying membrane-associated cytoskeleton. Both continuum and particle-based coarse-grained RBC models make use of a set of vertices connected by edges to represent the RBC membrane, which can be seen as a triangular surface mesh for the former and a spring network for the latter. Here, we present a modeling approach combining an existing continuum vesicle model with a coarse-grained model for the cytoskeleton. Compared to other two-component approaches, our method relies on only one mesh, representing the cytoskeleton, whose velocity in the tangential direction of the membrane may be different from that of the lipid bilayer. The finitely extensible nonlinear elastic (FENE) spring force law in combination with a repulsive force defined as a power function (POW), called FENE–POW, is used to describe the elastic properties of the RBC membrane. The mechanical interaction between the lipid bilayer and the cytoskeleton is explicitly computed and incorporated into the vesicle model. Our model includes the fundamental mechanical properties of the RBC membrane, namely fluidity and bending rigidity of the lipid bilayer, and shear elasticity of the cytoskeleton while maintaining surface-area and volume conservation constraint. We present three simulation examples to demonstrate the effectiveness of this hybrid continuum–coarse-grained model for the study of RBCs in fluid flows.

1. Introduction

The human red blood cells (RBCs) are normally biconcave discocytes with a diameter of approximately 8 μm and a thickness of about 2 μm. The mean volume is about 94 μm^3 and the average surface area around 135 μm^2, a value greater than the surface area of a sphere with the same volume. The RBC membrane (∼10 nm in thickness) is composed of a lipid bilayer supported from inside by a two-dimensional (2D) triangular spectrin network of cytoskeletal proteins. A highly elastic membrane, together with a high surface-to-volume ratio, provides RBCs with the ability of large reversible deformation when passing through capillaries. This composite bilayer–spectrin membrane may be treated as an elastic thin shell. Based on this simplified elastic description and the assumption of flat membrane, two fundamentally different approaches have

* Corresponding author.
E-mail addresses: gang.chen@univ-amu.fr (P.G. Chen), marc.jaeger@centrale-marseille.fr (M. Jaeger).

https://doi.org/10.1016/j.crme.2018.04.015

been proposed to study RBCs in fluid flows: one more traditional, founded on continuum mechanics, and the other, founded on molecular details, see for recent reviews [1–4].

The classical continuum approach, which was largely inspired by numerical methods developed in mechanical engineering, considers the suspending fluids as well as the RBC membrane itself as a continuous medium. A number of well-established continuum methods have been developed, including boundary integral/element method (BIM/BEM) and several interface tracking methods widely employed in multi-phase flows. These methods have been used to simulate the dynamics of a single RBC in flows as well as the collective behavior of an ensemble of them [4]. From this point of view, the RBC is most often modeled as a hyperelastic capsule (made of a polymerized membrane) [1,4]. However, the fluid nature of the cell membrane was systematically lacking; the near-incompressibility of the membrane was generally taken into account through a high dilatational modulus. Numerical simulations with vesicles (made of lipid bilayer) with bending rigidity can provide insight into the shapes taken by RBCs, either at equilibrium – the typical biconcave shape of RBCs or in flows – bullet, parachute and slipper shapes [1], but shear elasticity and shape memory that are the fundamental mechanical properties of RBCs are missing.

Discrete modeling exploits the microstructural properties of RBCs. Any medium is seen as a huge number of molecules, submitted to thermal agitation and to intermolecular forces. However, to be able to resolve much larger space and time scales involved in the transport of RBCs in fluid flows, coarse-graining of spectrin-level models has to be used, and the level of coarse-graining characterizes the crudeness with which the molecular level of the medium is represented [5]. Mesoscale (whole cell) particle-based methods [6] consider both the lipid bilayer and the spectrin cytoskeleton and the interaction between them. Some cell scale particle-based models keep the trace of the two contributions in the form of a two-component whole cell model [7,8]. In this way, the detachment of the cytoskeleton from the lipid bilayer, which for example can occur in the micropipet aspiration experience or in the flow through a constriction, has been successfully simulated [8].

One could regard the continuum approach as the ultimate state of coarse graining; however, in that ultimate state, the molecular structure is fully integrated and forgotten. There is a need for developing new numerical methods combining the two approaches, thus being able to benefit from advantages of both of them. Indeed, the idea of representing the cytoskeleton as a discrete 2D structure made of a large number of connected springs is very attractive. This is the starting point of the present contribution. Actually, particle-based and continuum-based models work all on the same principle: one mesh (or two coupled meshes if we distinguish between the bilayer and the cytoskeleton) made of triangular elements to represent the RBC membrane. In the particle-based model, the mesh is seen as a discrete network of springs, which tends to a good representation of the spectrin cytoskeleton when the number of vertices reaches the real cytoskeleton structure. In the continuum-based model, the mesh is understood as a finite element discretization of the membrane, in which a two-dimensional mesh, embedded in a 3D domain, is defined by a set of vertices connected by edges. Therefore, the same ingredients are present, providing very similar modeling possibilities in these two approaches.

In this paper, we propose to explore the idea whether the combination of a spring network with a vesicle model could give rise to an accurate and reliable hybrid discrete-continuum RBC model. It is a first attempt to couple a 3D vesicle model with a discrete description of the cytoskeleton. From purely mechanical considerations, such a model could extract the essential mechanical properties of the RBC membrane: fluidity and bending rigidity of the lipid bilayer, and shear elasticity of the cytoskeleton while maintaining surface-area and volume conservation constraint. This is also computationally feasible thanks to an existing continuum vesicle model [9,10]. The argument is that, in the vesicle model, the movements of the bilayer in the normal and tangential directions are treated differently, namely in Lagrangian fashion for the former and with an Eulerian description for the latter. Therefore the tangential movement of mesh vertices (or nodes in a finite element context), which does not change the membrane shape, is fully independent of the tangential movement of the lipids. Actually, the possibility of prescribing the tangential velocities of mesh vertices to any convenient set is used to preserve the mesh quality in a vesicle simulation context. Our idea for an extension towards RBCs is then to prescribe this velocity set to that of the vertices of a spring network. In doing so, the movement of the mesh vertices is constrained to slide along the bilayer. However, this constraint is automatically ensured by the fact that the same mesh is used both for the bilayer and the cytoskeleton, and that the nodes of the bilayer finite-element mesh are also the vertices connected by the edges of spring network. As far as numerical aspects are concerned, one of the major developments involves assigning a spring behavior law to the edges and a drag friction law (based on the lipid/node relative velocity) to the vertices, as well as a way how to incorporate these additional forces into the vesicle model.

In the following sections we first describe the RBC membrane model and outline the numerical methods. We then present three numerical examples to evaluate the proposed hybrid model, followed by a conclusion of the paper.

2. Cytoskeleton elasticity

The membrane model consists of a collection of points $\{\mathbf{x}_n, n \in 1 \dots N\}$, which are the vertices of the RBC surface triangulation, representing the cytoskeleton. The length of the link connecting vertices n and p is defined as $l_{np} = |\mathbf{x}_n - \mathbf{x}_p|$. The spring network induces on each node (or vertex) n of the surface mesh a resulting force given by

$$\mathbf{f}_n = \sum_p \mathbf{f}_{np} = \sum_p K_{np}(\mathbf{x}_p - \mathbf{x}_n) \tag{1}$$

where the summation is over all the vertices p connected to the node n by an edge np, i.e. spring np.

In Eq. (1), $\mathbf{f}_{np}$ denotes the force exerted by the node p on the node n, and K_{np} represents the stiffness coefficient of the spring np, connecting the node n at the position $\mathbf{x}_n$ to the node p at the position $\mathbf{x}_p$. In the case of a linear spring with the spring stiffness k_{np}, the force $\mathbf{f}_{np}$, as a function of the spring length l_{np} and its value at rest l^0_{np}, is given by

$$\mathbf{f}_{np} = k_{np}\frac{l_{np} - l^0_{np}}{l_{np}}(\mathbf{x}_p - \mathbf{x}_n) = k_{np}(1 - l^0_{np}/l_{np})(\mathbf{x}_p - \mathbf{x}_n) = K_{np}(\mathbf{x}_p - \mathbf{x}_n) \tag{2}$$

Since the aim of this paper is not to compare different spring laws but rather to test the idea described in the introduction, we only consider one of the constitutive laws proposed in [5], namely the finitely extensible nonlinear elastic (FENE) spring in combination with a repulsive force defined as a power function (POW). It is worth mentioning that compared to the linear spring model, i.e. Eq. (2), the FENE–POW spring model has been widely used for modeling the shear resistance of the cytoskeleton, especially for large deformations of RBCs [5]. The elastic energy of the spring np is then the sum of an attractive part and a repulsive one

$$U_{np} = -\frac{k_\mathrm{a}}{2}(l^{\max}_{np})^2 \log(1 - x^2_{np}) + \frac{k_\mathrm{r}}{(\alpha - 1)l^{\alpha-1}_{np}} \tag{3}$$

where k_a and k_r are, respectively, the FENE (attractive) and the repulsive spring constants, α is the repulsive exponent assumed as a constant value.

This expression uses the normalized spring length (or separation distance) $x_{np} = l_{np}/l^{\max}_{np} \in [0, 1]$. So, the spring's behavior law can be adjusted by fixing three physical parameters: the maximum spring length $l^{\max}_{np}$, and the attractive and repulsive spring constants k_a and k_r. The total stiffness coefficient K_{np} is given by

$$K_{np} = \frac{k_\mathrm{a}}{1 - x^2_{np}} - \frac{k_\mathrm{r}}{(l^{\max}_{np} x_{np})^{\alpha+1}} \tag{4}$$

Equation (4) defines a spring with non-zero equilibrium length l^0_{np} given by $\mathbf{f}_{np} = -\delta U_{np}/\delta \mathbf{x}_n = 0$ for $x^0_{np} = l^0_{np}/l^{\max}_{np}$. The equilibrium length l^0_{np} corresponds to the length of the spring in the reference shape, i.e. stress-free mesh. For simplification, we use hereinafter x_0 and l_0 to denote, respectively x^0_{np} and l^0_{np}. The two spring constants k_a and k_r can be related by

$$k_\mathrm{r} = k_\mathrm{a}\frac{l^{\alpha+1}_0}{1 - x^2_0} \tag{5}$$

Thanks to the Virial theorem, the elastic shear modulus of the spring network μ_S can be expressed in terms of k_a and k_r as follows:

$$\mu_\mathrm{S} = \frac{\sqrt{3}}{4}\left(\frac{2k_\mathrm{a}x^2_0}{(1 - x^2_0)^2} + \frac{k_\mathrm{r}(\alpha + 1)}{l^{\alpha+1}_0}\right) \tag{6}$$

Combining Eq. (4) with Eq. (5) and Eq. (6) yields finally the spring force at node n by an edge np

$$\mathbf{f}_{np} = K_{np}(\mathbf{x}_p - \mathbf{x}_n) = \frac{4\mu_\mathrm{S}}{\sqrt{3}\left(\frac{2x^2_0}{1-x^2_0} + \alpha + 1\right)}\left(\frac{1 - x^2_0}{1 - x^2_{np}} - \frac{x^{\alpha+1}_0}{x^{\alpha+1}_{np}}\right)(\mathbf{x}_p - \mathbf{x}_n) \tag{7}$$

As in [5], we set $\alpha = 2$ and the ratio $x_0 = 1/2.05$. For a given shear modulus μ_S, which is in the range of 4–12 μN/m for a normal RBC, and on the basis of the triangulation of cell membrane ($x_{np} = l_{np}x_0/l_0 = l_{np}x_0/l^0_{np}$) and its stress-free mesh ($l_0 = l^0_{np}$), the elastic force $\mathbf{f}^\mathrm{e}_{np}$ at node n by the edge np exerted by the spring network on the lipid bilayer can be obtained from Eq. (7) since $\mathbf{f}^\mathrm{e}_{np}$ is simply equal to $\mathbf{f}_{np}$, and subsequently incorporated into the bilayer–cytoskeletal interaction as described below.

3. Cytoskeleton–bilayer interaction

In [9,10], the boundary element method is used to resolve the lipid's flow on the vesicle membrane, which can be formulated as

$$\mathbf{u}^\mathrm{lip} = \mathbf{P}\left(\mathbf{u}^\infty + \mathbf{G}f^\mathrm{b}\right) \tag{8}$$

where the exponent "lip" stands for the lipid's velocity field and "∞" indicates the imposed background bulk fluid flow. **G** is the Green operator due to the Stokeslet, $f^{\mathrm{b}}(\mathbf{x})$ the bending force field induced by the lipid bilayer in response to deformations and **P** the projector onto a subspace of surface divergence-free vectors to satisfy the incompressibility constraint on the lipid's flow:

$$\mathrm{div}_S(\mathbf{u}^{\mathrm{lip}}) = 0 \tag{9}$$

The projector **P** includes the contribution of a surface-tension-like force resulting from the Lagrange multiplier of the surface divergence-free constraint.

In matrix form, it writes

$$\left[u_{n,i}^{\mathrm{lip}}\right] = [P]\left[u_{n,i}^{\infty}\right] + [P][G][F^{\mathrm{b}}(\mathbf{x})]\left[x_{n,i}(t+\mathrm{d}t)\right] \tag{10}$$

where the index "n, i" indicates the ith component of the position $\mathbf{x}_n$ or the velocity $\mathbf{u}_n$ of node n and $F^{\mathrm{b}}(\mathbf{x})$ is the matrix producing the nodal bending forces from the node positions (see [9] for details).

For a RBC, we have to add the elastic force $\mathbf{f}^{\mathrm{e}}$ exerted by the spring network on the lipid bilayer. It is given by a matrix $F^{\mathrm{e}}(\mathbf{x})$, which produces the nodal forces from the node positions in the same way as $F^{\mathrm{b}}(\mathbf{x})$ for bending. This spring elastic action is transmitted to the lipid bilayer in the normal direction directly and in the tangential plan indirectly via the drag forces $\mathbf{f}^{\mathrm{d}}$ that the lipids exert on the cytoskeleton

$$\mathbf{f}^{\mathrm{d}} = C_{\mathrm{f}}(\Pi_{\mathrm{tg}}\mathbf{u}^{\mathrm{lip}} - \Pi_{\mathrm{tg}}\mathbf{u}^{\mathrm{cyt}}) = \Pi_{\mathrm{tg}}\mathbf{f}^{\mathrm{e}} \tag{11}$$

where the exponent "cyt" stands for cytoskeleton and C_{f} is the friction coefficient. The operator $\Pi_{\mathrm{tg}} = Id - \Pi_n$ is the projector onto the tangent plan of the membrane surface, with $\Pi_n = \mathbf{n}\otimes\mathbf{n}$ the projector in the normal direction given by the normal vector **n** pointing toward the outside bulk fluid. Thus, the system (10) can be replaced by

$$\left[u_{n,i}^{\mathrm{lip}}\right] = [P]\left[u_{n,i}^{\infty}\right] + [P][G]\left([F^{\mathrm{b}}(\mathbf{x})] + ([\Pi_n] + [\Pi_{\mathrm{tg}}])[F^{\mathrm{e}}(\mathbf{x})]\right)\left[x_{n,i}(t+\mathrm{d}t)\right] \tag{12}$$

where $([\Pi_n] + [\Pi_{\mathrm{tg}}])$ can simply be eliminated, since it is nothing else than the identity matrix.

From the kinematic point of view, the sliding of the cytoskeleton is taken into account thanks to the mixed Lagrangian–Eulerian updating of the mesh node's position

$$\mathbf{x}(t+\mathrm{d}t) = \mathbf{x}(t) + \mathrm{d}t\,\mathbf{u} = \mathbf{x}(t) + \mathrm{d}t\,\Pi_n\mathbf{u}^{\mathrm{lip}} + \mathrm{d}t\,\Pi_{\mathrm{tg}}\mathbf{u}^{\mathrm{cyt}} \tag{13}$$

Thus, the mesh nodes moves with the lipid's velocity in the normal direction only, whereas it moves tangentially with the cytoskeleton's ones. Using equation (11), it writes also

$$\mathbf{x}(t+\mathrm{d}t) = \mathbf{x}(t) + \mathrm{d}t\,\Pi_n\mathbf{u}^{\mathrm{lip}} + \mathrm{d}t\,\Pi_{\mathrm{tg}}\mathbf{u}^{\mathrm{lip}} - \mathrm{d}t\frac{1}{C_{\mathrm{f}}}\Pi_{\mathrm{tg}}\mathbf{f}^{\mathrm{e}} = \mathbf{x}(t) + \mathrm{d}t\,\mathbf{u}^{\mathrm{lip}} - \mathrm{d}t\frac{1}{C_{\mathrm{f}}}\Pi_{\mathrm{tg}}\mathbf{f}^{\mathrm{e}} \tag{14}$$

or in matrix form

$$\left[x_{n,i}(t+\mathrm{d}t)\right] = \left[x_{n,i}(t)\right] + \mathrm{d}t\left[u_{n,i}^{\mathrm{lip}}\right] - \frac{\mathrm{d}t}{C_{\mathrm{f}}}[\Pi_t][F^{\mathrm{e}}(\mathbf{x})]\left[x_{n,i}(t+\mathrm{d}t)\right] \tag{15}$$

Using the Stokes–Einstein relation and measured values of the translational diffusivity of band 3 and glycophorin C in the lipid bilayer, the drag force and thus the values of the friction coefficient can be deduced [11]. However, these values are relevant only in the context of a spectrin-scale modeling or in the case involving a dynamical process. In the present study, the value of C_{f} affects only numerical efficiency; $C_{\mathrm{f}} \to 0$ is equivalent to minimizing the elastic energy at each time step, whereas a finite value leads to a relaxation of the cytoskeleton stresses. We set $C_{\mathrm{f}} = 1$ in most of our computations, but the final stationary RBC shape remains the same for all the examples we have considered, whatever its value.

4. Numerical examples

Here, we present three simulation examples to evaluate the proposed approach.

(i) Sedimentation of an initially prolate vesicle in an infinite fluid for increasing values (μ_S) of spring forces. In this way, we can get insight into how the presence of a discrete spring network, representing the cytoskeleton, alters the large deformation of a settling vesicle. Since our approach is based on a combination of a vesicle model with a cytoskeleton, it is natural to begin with this relatively simple case. Another reason is that the case of a settling vesicle exhibiting a finger-like protuberance has been extensively studied over the past years, which enabled us to start from well-validated stationary vesicle shapes [9,10,12].
(ii) Stretching of a RBC in the optical tweezers experiment [13], which is a more classic validation of RBC models.
(iii) Motion of a single RBC in a capillary.

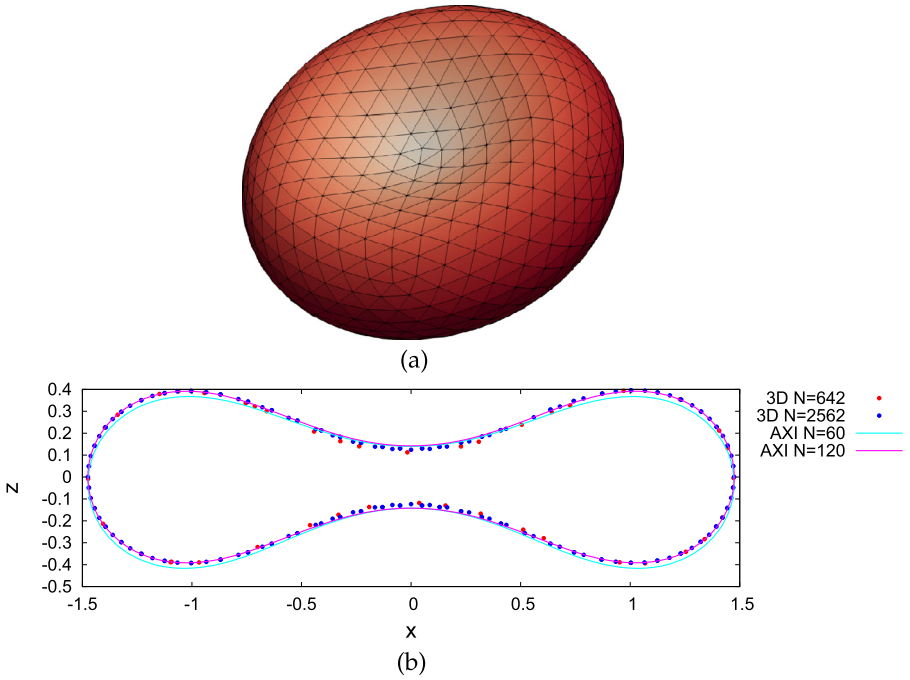

Fig. 1. (a) Final discoidal shape of a simulated three-dimensional vesicle with $v = 0.6$ (typical value for RBCs). The triangular mesh is composed by $N = 642$ nodes and $M = 1280$ elements. The mesh is constructed by refining the triangular faces of an icosahedron inscribed into a sphere by dividing recursively each triangle into four smaller triangles, and projecting the resulting nodes to the surface of the sphere. (b) A comparison of the final shapes for increasing mesh elements, both in the 3D and in the axisymmetric case.

A surface mesh of $M = 1280$ triangular elements, as shown in Fig. 1(a), is typically used in our numerical simulations. The discoidal shape obtained from the stress-free state of a vesicle is used as a reference shape; it defines the equilibrium position of the nodes and the equilibrium length of the spring network that simulate the spectrin network of the cytoskeletal proteins. However, it must be stressed that there is no universal consensus on the reference shape that should be adopted to describe the real deformation of a RBC under external solicitations. Fig. 1(b) shows a comparison between the stationary shapes obtained by the 3D code and the axisymmetric one for a vesicle with the same deflation $v = 0.6$ of a RBC. In both the axisymmetric and the three-dimensional cases, a convergence towards the final shape is observed when increasing the number of mesh elements. The first feature we notice is that a good description of the 3D final vesicle shape can be obtained, even with a relatively small number of triangular elements.

The shear modulus is defined by $\mu_S = c\mu_0$, with $\mu_0 = 5$ μN/m as a reference value for the shear stress of a healthy RBC cytoskeleton, and then we let μ_S vary through the coefficient c to adjust the strength of the cytoskeleton contribution; $c = 0$ corresponds to a purely vesicle model, whereas $c = 1$ leads to a two-component vesicle–cytoskeleton model; increasing this coefficient results, as expected, in an increase in the shear resistance of the cell membrane.

Before presenting the numerical results, it is useful to recall some relevant dimensionless parameters that we are using. If the vesicle has a volume V $(= 4/3\pi R_0^3$, which defines a characteristic vesicle size $R_0)$ and a surface area A, then the vesicle motion, as it flows in a circular capillary, is determined by three independent dimensionless parameters:

(1) the reduced volume v $(= 3\sqrt{4\pi}V A^{-3/2}$, which quantifies the geometric ability of the vesicle to deform, it can range from 0 – totally deflated vesicle – to 1 – sphere. RBCs have a typical value between 0.6 and 0.65);
(2) the bending capillary number Ca $(= \eta U R_0^2/\kappa_B$, where κ_B is the bending modulus, η the viscosity of ambient fluid, and U the maximum velocity of unperturbed Poiseuille flow);
(3) the confinement parameter β $(= R_0/R_c)$ between the vesicle size R_0 and the capillary radius R_c.

In the case of buoyant vesicles, a new dimensionless parameter is introduced to compare gravitational energy to bending energy, the Bond number Bo $(= \Delta\rho g R_0^4/\kappa_B$, where $\Delta\rho$ is the difference of density between inner and outer fluids, g the gravity). When taking into account the shearing resistance of the cell membrane, we need to define another non-dimensional parameter, called the reduced bending number C_b, which is the ratio of the bending modulus to the shearing modulus, $C_b = \kappa_B/(\mu_S R_0^2)$. We have $C_b \approx 0.005$ for RBCs if we set $\kappa_B = 2.4 \times 10^{-19}$ J [5,7], $R_0 = 3$ μm, and $\mu_S = 5$ μN/m [5,7]. These values are used in our simulations when appropriate, despite a large scatter in the experimentally measured values.

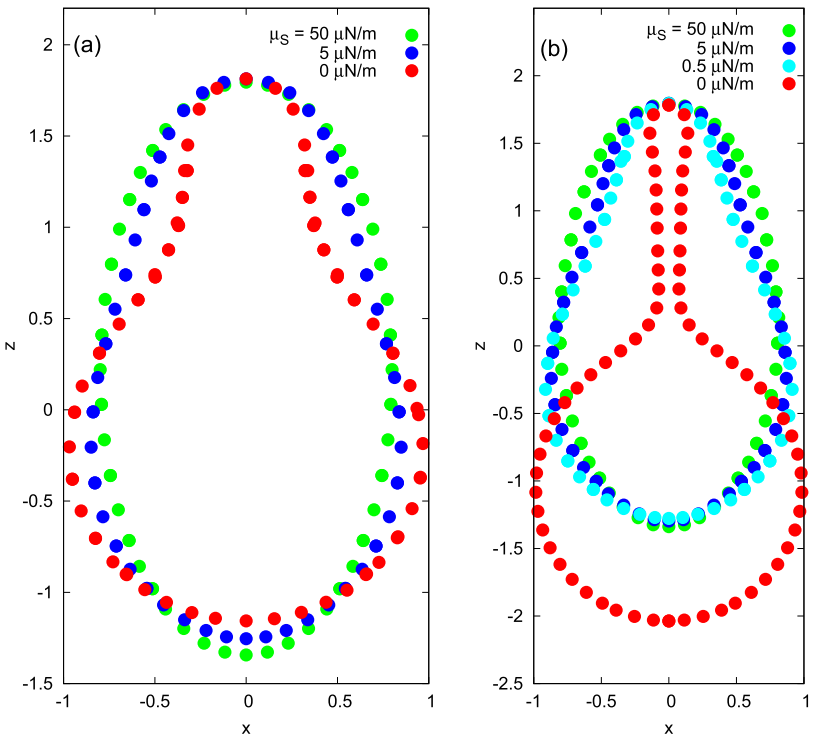

Fig. 2. Stationary shape profiles of a vesicle–cytoskeleton model with reduced volume $v = 0.9$ for several values of c and of the Bond number in the sedimentation simulations. (a) $Bo = 40$, (b) $Bo = 220$. In the case of a vesicle ($\mu_S = 0$ μN/m), there is a finger-like shape that disappears if we increase the value of the shear modulus μ_S. For high values of the shear modulus ($\mu_S > 50$ μN/m), the final shape is close to the initial reference one – a prolate ellipsoid. Coordinates are normalized with the equivalent radius of the vesicle R_0.

4.1. Sedimentation

The first simulation example deals with a settling vesicle in combination with an underlying discrete spring network in an unbounded flow. Our objective here is to evaluate how effectively a cytoskeleton can influence the final shape of a settling vesicle. The appropriate dimensionless parameters involved are the reduced volume v, the Bond number Bo, and the reduced bending number C_b. Instead of using C_b, we explicitly prescribe the value of c ($\mu_S = c \times 5$ μN/m), and thus study the sedimentation of an initially prolate shape of fixed reduced volume for different values of the Bond number. We investigate the influence of the spring forces on the final shape in order to better characterize our model for the simple case of the gravity-induced sedimentation of a vesicle. We intentionally set very high values of the Bond number so that the vesicle exhibits large deformations characterized by the emergence of a stationary long finger-like shape. If we neglect the action of the cytoskeleton, the corresponding final shape is the same as when the vesicle has the same deflation and Bond number. We compare the deformation of the final shape for increasing network connecting forces. A prolate ellipsoid with $v = 0.9$ is selected as the reference shape (i.e. stress-free state); we perform several simulations for different values of μ_S for a given Bo. We observe that, for high values of μ_S, the membrane does not deform because the cytoskeleton elastic force is too high and the final shape comes back to the initial reference one. For low values of μ_S, the final shape is close to the stationary shape of a settling vesicle with same values of v and Bo.

Numerical results are presented in Fig. 2, where the axisymmetric stationary shape profiles for increasing values of c are compared to that of a vesicle (i.e. $\mu_S = 0$ μN/m). An initially prolate shaped vesicle of reduced volume 0.9 evolves towards a pear like shape with an elongated tail all the more pronounced when the Bond number becomes higher. It makes it clear that the presence of a cytoskeleton prevents such large deformations. Even a small value of μ_S (0.5 μN/m) can maintain the shape close to the initial prolate in a sedimentation experiment for reasonable values of the Bond number. From this numerical experience, it is concluded that the emergence of long finger-like shapes can be observed only for vesicle sedimentation, since in the case of RBCs, even for large values of Bo, the cytoskeleton prevents the finger from appearing, indicating a significant interplay between vesicle dynamics and the cytoskeleton.

4.2. RBC stretching

As a second numerical example, we perform RBC stretching simulations and compare our numerical results with the experimental data of RBC deformations by optical tweezers [13]. In our simulations, the reference shape of RBC is a biconcave surface, and the geometry can be obtained using the following expression [14]

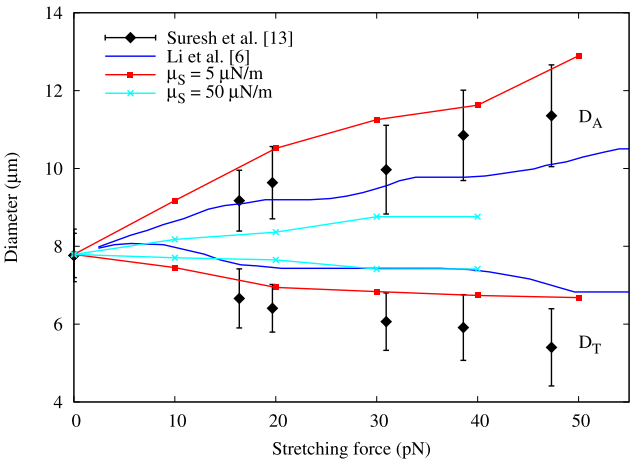

Fig. 3. Variation of the axial D_A and transverse D_T diameter (μm) of RBC membrane as a function of stretching forces (pN) for two values of the shear modulus, $\mu_S = 5$ μN/m and $\mu_S = 50$ μN/m. Simulation results are compared with the optical-tweezers experiment [13] and numerical predictions by a spectrin-level modeling [6].

$$z = \pm D\sqrt{1 - \frac{4(x^2+y^2)}{D^2}}\left[a_1 + a_2\frac{x^2+y^2}{D^2} + a_3\frac{\left(x^2+y^2\right)^2}{D^4}\right] \tag{16}$$

where $D = 7.82$ μm is the cell diameter, $a_1 = 0.0518$, $a_2 = 2.0026$ and $a_3 = -4.491$. The volume and surface area of the corresponding RBC are respectively 94 μm^3 and 135 μm^2, giving a reduced volume $v = 0.64$.

The RBC membrane network is composed of N vertices, which define the level of the membrane representation from the spectrin-level to the coarse-grained network of N (= 642). The total stretching force F_s is applied to N_- ($-F_s$) and N_+ ($+F_s$) vertices, with $N_- = N_+ = \epsilon N$, along the negative and positive axial directions, respectively. These vertices cover a near-spherical area on the surface with $\epsilon \approx 0.02$, which is in agreement with the contact area of the attached silica bead with diameter $d_c \approx 2$ μm used in the experiments. The axial diameter D_A is computed as $|x_{\max} - x_{\min}|$, where $x_{\max}$ is the maximum x position among the N_+ vertices and $x_{\min}$ is the minimum one among the N_- vertices. The transverse diameter D_T is calculated as $2 \times \max_{i=1\ldots N}\sqrt{(y_i - c_y)^2 + (z_i - c_z)^2}$, where c_y and c_z are the coordinates of the y and z centers of mass.

The elastic shear modulus μ_S measured experimentally lies in the range of 4–12 μN/m, and the bending modulus in the range of $1\text{–}7\times10^{-19}$ J [5,7], indicating a large-amount scatter in the measured values. Fig. 3 shows the change in RBC's axial and transverse diameters in response to the applied stretching forces. As the stretching force increases, the RBC's axial diameter increases, while the transverse one decreases from the initial value $D = 7.82$ μm. We find a reasonable good agreement with the experimental data of RBC deformation when we set $c = 1$, i.e. $\mu_S = 5$ μN/m, given the uncertainty in the measured mechanical properties of the RBC membrane. For a much higher value of μ_S, i.e. $\mu_S = 50$ μN/m, the RBC membrane withstands significantly the applied stretching forces since the cell deformation is much less. As could be expected, the deformations of the RBC membrane in response to the applied stretching forces depend largely on the value of the shear modulus used in a numerical model. Indeed, the finite element method simulation of the RBC membrane [13] finds an agreement with the experimental data for $\mu_S = 5.3$ μN/m, whereas Fedosov et al. [5] obtain a better agreement for $\mu_S = 6.3$ μN/m. Our simulation results are also fully consistent with the numerical results reported in [6]. Based on spectrin-level modeling, Li et al. [6] obtained an inferred value of the shear modulus $\mu_S = 8.3$ μN/m – a relatively higher value of the shear modulus than that we used in the simulations, which could explain why our model gives rise to a relatively larger deformation of the RBC membrane when compared to that predicted by Li et al. [6].

While our model offers an important advantage in the case of hydrodynamic solicitations typical of sedimentation dynamics thanks to the inclusion of a fluid solver, the model, in its current implementation, suffers from difficulties in larger, sharp solicitations such as in the "optical tweezers" experiment. When the applied stretching force of F_s is higher than 60 pN, the induced forces within the spring network are too strong compared to the most common hydrodynamic forces, which is the prelude to the possibility of increasing further the loading force. A possible solution to this problem can be the implementation of a more efficient relaxation algorithm and/or the use of a locally mesh-refinement strategy. It is worth mentioning that there is a tremendous difference in the number of vertices being used between a spectrin-level RBC modeling and a coarse-grained model; the former uses about 30,000–40,000 vertices, and the latter, such as ours, uses around 500–1,000 vertices.

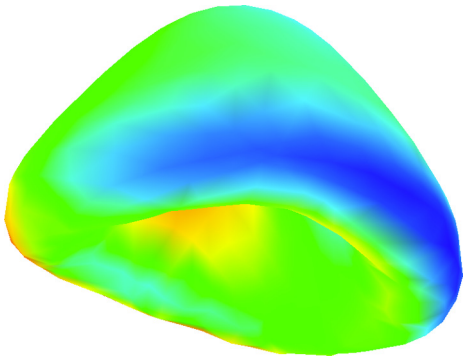

Fig. 4. Three-dimensional shape of a vesicle having the same typical deflation of a RBC (i.e. $\nu = 0.6$) immersed in a capillary with $\beta = 0.5$ and $Ca = 10$. The colors represent the intensity of the surface divergence of velocity on the vesicle (Eq. (9)), which is on the order of 10^{-9} (blue)$\sim 10^{-8}$ (red), an indication of the near-incompressibility of the membrane.

4.3. Motion of a single RBC in a capillary

The third and the last simulation example concerns a single RBC in capillary flows. For practical issues, the transport of BRCs inside a capillary is a more relevant situation to consider. Two specificities of this class of flows contribute to RBC deformation: curvature of the Poiseuille-type flow profile and confinement. For large capillaries, the RBC sees the influence of the boundaries only through the background velocity profile (typically Poiseuille flow). Direct interaction with a wall appears only for the RBC coming very close to it. For small capillaries, the RBC feels the direct influence of the walls from all sides. Thus, it feels that wall not only through the action on the velocity profile, but also directly through the confinement effect, and thus both the curvature of the flow and the confinement become involved. The confinement is characterized by the confinement parameter β; a larger value of β means a stronger confinement. The strength of the flow and its relative importance with respect to the bending energy is characterized by the capillary number Ca.

As in the case of sedimentation in an unbounded flow, we analyze the differences between the final shape of a vesicle and a RBC for increasing strengths of the spring network. Fig. 4 shows the equilibrium shape of a vesicle with the same deflation as that of a RBC ($\nu = 0.6$) submitted to a Poiseuille flow inside a capillary for $\beta = 0.5$ and $Ca = 10$. The final shape is a non-axisymmetric parachute. Indeed, if the confinement is not strong enough, non-axisymmetric vesicle shapes could be observed. They become axisymmetric when the confinement is increased beyond a critical value, which strongly depends on other control parameters. Since the most significant challenge in vesicle dynamics simulations is to require and enforce an incompressibility constraint of the membrane surface, locally and globally, the field of surface divergence of velocity is shown on the vesicle.

The influence of the presence of a cytoskeleton on the shape taken by the cell is illustrated in Fig. 5 for $Ca = 10$ and $\beta = 0.33$ (top left) or $\beta = 0.5$ (bottom left). A vesicle (red profiles) takes a typical parachute-like shape whose curvature increases with confinement and which can deviate from the axial symmetry, as shown in Fig. 5 by the difference in the xy and xz cross sections (filled and unfilled circles). When the effect of a cytoskeleton is considered, even for a very weak shear modulus ($\mu_S = 0.5$ μN/m), large deformations of the parachute shape are reduced substantially, and the asymmetry of the cell becomes less significant. As the cytoskeleton strength is further increased ($\mu_S = 5$ μN/m) the cell recovers the discocyte shape typical of RBCs at rest. That means that hydrodynamic forces are not strong enough to oppose to cytoskeletal forces in order to allow shape deformation, and that the biconcave shape is more resistant to the flow stress.

The choice of the reference shape assume an increasing importance on the final shape for high values of μ_S. Therefore, it would be interesting to extend the study by considering different reference shapes. Another remark concerns the accuracy of the state of the cytoskeleton, which shows local anomalous surface features (hills) in equilibrium (Fig. 5-bottom right) when the shearing resistance becomes larger, though it seems to be less pronounced with a mesh refinement. This feature has also been reported in [5], leading them to try to overcome the difficulty with the help of an appropriate numerical treatment. Such a strategy would involve a significant computational effort to account for larger deformations of RBCs in narrow capillaries.

5. Conclusion

By combining a continuum description of a lipid membrane with a discrete representation of cytoskeleton, we have presented an approach for modeling the membrane of red blood cells in the context of the prediction of red blood cells dynamics in a flow. The model includes the essential mechanical properties of the RBC membrane, namely shearing resistance and bending rigidity, as well as the constraints of fixed surface area and fixed enclosed volume. Specifically, the RBC membrane is modeled as a composite network, which consists of a dynamically triangulated surface as in a fluid vesicle model. The membrane is then coupled with an additional network of springs with fixed connectivity, representing the cytoskeleton. Compared to other two-component approaches, we explicitly computed the mechanical interaction between the bilayer and

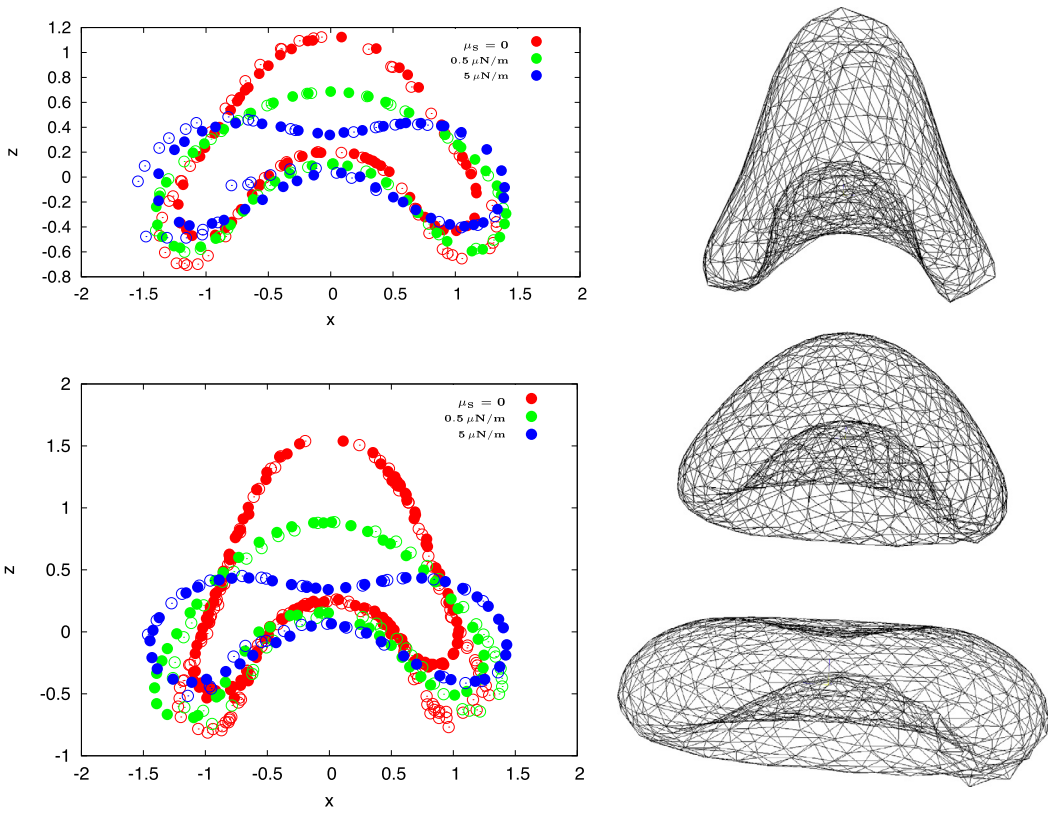

Fig. 5. Stationary shape profiles obtained with the two-component vesicle–cytoskeleton model for a RBC transported in a capillary for increasing contribution of cytoskeleton, $Ca = 10$ and two confinement parameters: $\beta = 0.33$ (top left) and $\beta = 0.5$ (bottom left). Filled and unfilled circles represent the cross sections on the xz and yz plane, respectively. Coordinates are normalized with the equivalent radius of the RBC. The finite-element meshes, i.e. the state of the cytoskeleton corresponding to the shape profiles for $\beta = 0.5$ are shown on the right.

the cytoskeleton by considering normal elastic spring and tangential friction force. Another advantage is only one mesh that is used both for the bilayer and the cytoskeleton, thus significantly reducing the computational complexity.

We have presented three simulation examples to illustrate the effectiveness of our model. As the aim of this work was to see if adding a spring network to a BEM vesicle model could be a possible way to build a RBC model, we have thus focused our attention on the main issue, namely the capacity of the model to handle the shape memory effect of a cytoskeleton, especially in the case of large deformations such as the sedimentation case with a large Bond number. We have therefore limited our study to stationary shapes; a full model accounting for a real friction coefficient between the bilayer and the cytoskeleton has not been tested. The tank-treading motion of RBCs in a shear flow [11] represents an interesting test to examine the extent to which our model deals with dynamical behaviors. Given the essential ingredients that are already present in our model, there is no obvious reason why our model should fail to capture the dynamical behaviors of a tank-treading case, which would involve merely an actual value of the friction coefficient between the bilayer and the cytoskeleton of the RBC membrane, instead of an arbitrarily chosen value for stationary shapes.

This work fills the gap between continuum mechanical modeling and coarse-grained modeling of RBC membranes by fusing these two approaches. Our numerical results show that this two-component vesicle–cytoskeleton model is able to extract the mechanical properties of RBCs and predict its dynamics in fluid flows. However, our model in its current implementation suffers from difficulties in high, local mechanical loading such as in the tweezers experiment. A solution to overcome this problem is to use locally a mesh-refinement strategy. Another problem relates to the accuracy of the state of cytoskeleton, which showed local anomalous surface features (kinks). We need to use a suitable numerical treatment to mitigate this issue. Moreover, further investigation is needed to consider different reference shapes of the cytoskeleton that should be adopted in order to provide deeper insights into the dependence of the stationary shape on the reference one for different flow configurations. A more performing algorithm for the computation of the cytoskeleton interactions and for the energy minimization would also be welcomed.

Acknowledgements

We acknowledge financial support from Labex MEC (grant No. ANR-11-LABX-0092), from A*MIDEX (grant No. ANR-11-IDEX-0001-02) and from CNES. J.M. Lyu is sponsored by China Scholarship Council (CSC). This work was granted access

to the HPC resources of Aix–Marseille Université financed by the project Equip@Meso (ANR-10-EQPX-29-01). We thank an anonymous referee for his/her thorough review and detailed constructive suggestions, which allowed us to improve the paper.

References

[1] P.M. Vlahovska, T. Podgorski, C. Misbah, Vesicles and red blood cells in flow: from individual dynamics to rheology, C. R. Physique 10 (2009) 775–789.
[2] P.M. Vlahovska, D. Barthes-Biesel, C. Misbah, Flow dynamics of red blood cells and their biomimetic counterparts, C. R. Physique 14 (2013) 415–459.
[3] X. Li, P.M. Vlahovska, G.E. Karniadakis, Continuum- and particle-based modeling of shapes and dynamics of red blood cells in health and disease, Soft Matter 9 (2013) 28–37.
[4] J.B. Freund, Numerical simulation of flowing blood cells, Annu. Rev. Fluid Mech. 46 (2014) 67–95.
[5] D.A. Fedosov, B. Caswell, G.E. Karniadakis, Systematic coarse-graining of spectrin-level red blood cell models, Comput. Methods Appl. Mech. Eng. 199 (2010) 1937–1948.
[6] J. Li, M. Dao, C.T. Lim, S. Suresh, Spectrin-level modeling of the cytoskeleton and optical tweezers stretching of the erythrocyte, Biophys. J. 88 (2005) 3707–3719.
[7] H. Noguchi, G. Gompper, Shape transitions of fluid vesicles and red blood cells in capillary flows, Proc. Natl. Acad. Sci. USA 102 (2005) 14159–14164.
[8] X. Li, Z. Peng, H. Lei, M. Dao, G.E. Karniadakis, Probing red blood cell mechanics, rheology and dynamics with a two-component multi-scale model, Philos. Trans. R. Soc. Lond. A 372 (2014) 20130389.
[9] G. Boedec, M. Leonetti, M. Jaeger, 3D vesicle dynamics simulations with a linearly triangulated surface, J. Comput. Phys. 230 (2011) 1020–1034.
[10] R. Trozzo, G. Boedec, M. Leonetti, M. Jaeger, Axisymmetric boundary element method for vesicles in a capillary, J. Comput. Phys. 289 (2015) 62–82.
[11] Z. Peng, R.J. Asaro, Q. Zhu, Multiscale modeling of erythrocytes in Stokes flow, J. Fluid Mech. 686 (2011) 299–337.
[12] G. Boedec, M. Jaeger, M. Leonetti, Settling of a vesicle in the limit of quasispherical shapes, J. Fluid Mech. 690 (2012) 227–261.
[13] S. Suresh, J. Spatz, J.P. Mills, A. Micoulet, M. Dao, C.T. Lim, M. Beil, T. Seufferlein, Connections between single-cell biomechanics and human disease states: gastrointestinal cancer and malaria, Acta Biomater. 1 (2005) 15–30.
[14] E.A. Evans, R. Skalak, Mechanics and Thermodynamics of Biomembranes, CRC Press Inc., Boca Raton, FL, USA, 1980.